SNPP VIIRS Polarization Sensitivity Analysis

Junqiang Sun[1,2], Xiaoxiong Xiong[3], Eugene Waluschka[3], and Menghua Wang[1]

[1]NOAA National Environmental Satellite, Data, and Information Service
Center for Satellite Applications and Research
E/RA3, 5830 University Research Ct.
College Park, Maryland 20740, USA

[2]Global Science and Technology, 7855 Walker Drive, Suite 200, Maryland, USA

[3]Sciences and Exploration Directorate, NASA/GSFC, Greenbelt, MD 20771

ABSTRACT

The Visible Infrared Imaging Radiometer Suite (VIIRS) is one of five instruments onboard the Suomi National Polar-orbiting Partnership (SNPP) satellite that launched from Vandenberg Air Force Base, California, on October 28, 2011. It is a whiskbroom radiometer that provides ±56.28° scans of the Earth view (EV). It has 22 bands, among which 14 are Reflective Solar Bands (RSB). The RSB cover a wavelength range from 410 to 2250 nm. The RSB of a remote sensor are usually sensitive to the polarization of incident light. For VIIRS, it is specified that the polarization factor should be smaller than 3% for 412nm and 862nm bands and 2.5% for other RSB for the scan angle within ±45°. Several polarization sensitivity tests were performed prelaunch for SNPP VIIRS. The first few tests either had large uncertainty or were less reliable, while the last one was believed to provide the more accurate information about the polarization property of the instrument. In this paper, the measured data in the last polarization sensitivity test are analyzed and the polarization factors and phase angles are derived from the measurements for all the RSB. The derived polarization factors and phase angles are band, detector, and scan angle dependent. For near-infrared bands, they also depend on half angle mirror (HAM) side. Nevertheless, the derived polarization factors are all within the specification although the strong detector dependence of the polarization parameters was not expected. Compared to the Moderate Resolution Imaging Spectroradiometer (MODIS) on both Aqua and Terra satellites, the polarization effect on VIIRS RSB is much smaller.

Keywords: SNPP, VIIRS, Polarization, Reflective Solar bands, Calibration, MODIS

I. INTRODUCTION

The Visible Infrared Imaging Radiometer Suite (VIIRS) is one of five instruments onboard the Suomi National Polar-Orbiting Partnership (SNPP) satellite that launched from Vandenberg Air Force Base, California, on October 28, 2011 [1]. The VIIRS is a whiskbroom radiometer that views the entire Earth surface approximately daily using a rotating telescope assembly and a double-sided half-angle mirror with a swath of 3060 km cross track by 12 km along track (at nadir) each scan [2]. VIIRS has 22 spectral bands, among which are 14 reflective solar bands (RSB) with wavelengths ranging from 410 to 2250 nm. The wavelengths of the VIIRS RSB are listed in the second row in Table 1. Among the 14 RSB, 3 are image bands with 32 detectors each and 11 are moderate spatial resolution bands with 16 detectors each. The RSB are calibrated on-orbit using a Solar Diffuser (SD) with a Solar Diffuser Stability Monitor (SDSM) and near-monthly lunar observations [3-10]. Figure 1 is a schematic diagram for VIIRS and its on-board calibrators. In the calibration methodologies, the incident light is assumed to be unpolarized and, thus,

both the SD/SDSM calibration and the lunar calibration can only provide the calibration coefficients for the RSB in the case when the incident light is unpolarized. It is known that the Visible and Near InfraRed (VisNIR) bands, the major component of the RSB, of a whiskbroom radiometer are sensitive to polarization of the incident light, especially the short wavelength bands, and the sunlight reflected from the earth surface is in fact polarized [11]. The polarization of the reflected sunlight is scene dependent and the sunlight can be strongly polarized at various regions on the earth surface [12, 13]. Therefore, it is critical to correct the polarization effect in the instrument Earth view radiance in order to get accurate Environmental Data Records (EDR) [14]. To correct the effect, the polarization sensitivity of the VisNIR bands needs to be well characterized [15].

The polarization property of a VisNIR band is described by two parameters, a polarization factor and a polarization phase angle [11]. The polarization sensitivity is characterized by the polarization factor. It is one of the key specifications for the VisNIR bands of a remote sensor and one of the major concerns when the sensor is designed and built [16, 17]. For SNPP VIIRS VisNIR bands, the polarization sensitivity is required to be less than 3% for bands M1, I2, and M7 and less than 2.5% for all other VisNIR bands for the scan angle, shown in Figure 2, within $\pm 45^{o}$ [16]. The polarization sensitivity specification for each of the VIIRS VisNIR is also listed in the third row in Table 1. The polarization sensitivity of a remote sensor is characterized on ground using the prelaunch measurement with a linearly polarized light source. The instrument response change with the orientation of the polarization direction of the incident light provides the information of the instrument's polarization sensitivity. The uncertainty of the polarization sensitivity measurements strongly depends on the uniformity of the light source with respect to the rotation of the polarization direction. For SNPP VIIRS, the uncertainty of polarization sensitivity characterization is specified to be less than 0.5% [16].

Several tests were conducted to examine the sensitivity of the SNPP VIIRS, which was called VIIRS Flight Unit 1 (FU1) during the prelaunch measurements of the instrument, to linearly polarized light and to measure polarization sensitivity for each VisNIR band and detector. The measured data of these tests have been carefully analyzed to characterize the polarization properties of the VIIRS FU1 VisNIR bands [18-21]. There are two types of tests. In the first type of tests, a Polarization Source Assembly (PSA) was used to provide polarized incident light. It was shown from the data analysis that the PSA could not provide uniform polarized incident light for the test and the uncertainty due to the non-uniformity and other noise was larger than 0.5%, exceeding the specified characterization uncertainty [18]. In the second type of tests, the polarized light was provided by the Spherical Integration Source (SIS) with a polarizer sheet. The tests of second type can be further separated as pre-TV (Thermal Vacuum) tests, STR-545 and STR-554, and post-TV test, ETP-679. In the pre-TV tests, the polarizer sheets used in the measurements were not perfectly polarized and the tests were also implemented only for a few selected bands [19]. In the post-TV test, the polarization degree of the polarizer sheets used in the test was examined first and all the VisNIR bands were covered in this test. In this test, the flaws or limitations in previous tests were removed [20]. This test provided a complete measurement of the polarization sensitivity of the instrument.

In this paper, we analyze the measured data of the post-TV test and derive polarization parameters for SNPP VIIRS VisNIR bands. In section 2, we give a theoretical description of the polarization analysis and a detail formulation of the correction of the polarization effect in the Earth View (EV) radiance or reflectance of a VisNIR band. In section 3, we analyze the data and derive the polarization parameters. In section 4, we analyze the derived polarization parameters and derive the Look Up Tables (LUT), which are used in real applications. The detector, wavelength and scan mirror side dependence of the polarization parameters are examined and analyzed. We also compare the polarization sensitivity of the SNPP VIIRS to those of the MODIS instruments [11]. In section 5, a summary concludes this analysis.

II. THEORY AND ALGORITHM

A. Polarization Formulism

A monochromatic linear polarized light beam can be described by a plane wave. With **E** being the electric field of the light, then the radiance of the light can be written as [22]

$$I = \mathbf{E}^{\dagger}\mathbf{E}, \tag{1}$$

where $\mathbf{E}^{\dagger}$ is the conjugate transpose of **E**. When the light passes through an optical system, the electric field at each optical surface changes and at the detector the beam of light $\mathbf{E}'$ can be related to the incident electric field **E** by a two dimensional Jones matrix **U [23]** by

$$\mathbf{E}' = \mathbf{U}\mathbf{E}. \tag{2}$$

The radiance of the light reaching the detectors on the focal plane of the instrument is then given by

$$I' = \mathbf{E}^{\dagger}\mathbf{H}\mathbf{E}, \tag{3}$$

where

$$\mathbf{H} = \mathbf{U}^{\dagger}\mathbf{U} \tag{4}$$

is a two-dimensional Hermitian matrix. For a coordinate system with z-axis pointing along the direction of propagation as shown in Figure 3a, the electric field vector of the linear polarized light can be written as

$$\mathbf{E} = \begin{pmatrix} \cos(\alpha) \\ \sin(\alpha) \end{pmatrix} E, \tag{5}$$

where E is the amplitude of the electric field, α is the angle between the direction of the electronic field and in Fig.3 the x-axis and called polarization angle. For a remote sensor, such as VIIRS, it is reasonable to assume that the Hermitan matrix **H** is a real matrix and that it can be expressed as [11]

$$\mathbf{H} = h\begin{pmatrix} \cos(\delta) & -\sin(\delta) \\ \sin(\delta) & \cos(\delta) \end{pmatrix}\begin{pmatrix} 1+a & 0 \\ 0 & 1-a \end{pmatrix}\begin{pmatrix} \cos(\delta) & \sin(\delta) \\ -\sin(\delta) & \cos(\delta) \end{pmatrix}, \tag{6}$$

where h is the averaged transmittance of the optical system, a is called the polarization factor, and δ is called the polarization phase angle which may change with the coordinate system. The transmittance of the optical system varies with the direction of electric field vector of the polarized light and the polarization phase angle specifies the direction for the maximum transmittance as displayed in Figure 3b. By substituting Eq. (6) into Eq. (3), we can express the radiance as [11]

$$I' = hI\{1 + a\cos[2(\alpha - \delta)]\}. \tag{7}$$

The power finally reaching the detectors on the focal plane of the instrument varies with the polarization angle. Although both α and δ change with the coordinate system, the difference between α and δ is independent of the coordinate system.

An unpolarized light has a random distribution of its electric filed in the plane perpendicular to the direction of propagation. Light from nature such as sunlight is unpolarized light. However, sunlight reflected from the Earth surface can become polarized due to Rayleigh scattering, surface reflection, and other effects. The electric field of the reflected sunlight may have a large component in one direction while less in other directions. In this partially polarized light case, there is a direction in the plane perpendicular to its direction of propagation, in which the electric field has the largest distribution as shown in Figure 3c. Let μ be the angle between this direction and the x-axis, I_1 be the total radiance of the light projected along the maximum direction and I_2 be the total radiance projected on the perpendicular direction, then the final radiance passing through the optical system can be written as [11]

$$I' = hI\{1 + fa\cos[2(\mu - \delta)]\}, \tag{8}$$

where

$$f = \frac{I_1 - I_2}{I_1 + I_2} \tag{9}$$

is the scene polarization factor that measures the degree of polarization of the incident light.

An alternative approach to describe the polarized light, especially partially polarized light is using the Stokes vector [24, 25]

$$\mathbf{I} = \begin{pmatrix} I \\ Q \\ U \\ V \end{pmatrix}, \tag{10}$$

where

$$I = \left\langle E_x^* E_x + E_y^* E_y \right\rangle,\ Q = \left\langle E_x^* E_x - E_y^* E_y \right\rangle,\ U = \left\langle E_x^* E_y + E_x^* E_y \right\rangle,\ V = \left\langle E_x^* E_y - E_y^* E_x \right\rangle, \tag{11}$$

E_x and E_y are the components of the electric field in x- and y-axis, the superscript asterisk indicates the complex conjugate, and the angle bracket denotes the average over time. The first component of the Stoke vector is the radiance of the light as same as that expressed in Eq. (1). The effect of the optical system on the Stoke vector **I** is described by a Mueller matrix, i.e. the Stoke vector, **I***'*, for the light passing the optical system can be written as

$$\mathbf{I}' = \mathbf{M}\mathbf{I}, \tag{12}$$

where **M** is a 4×4 matrix. Then the radiance reaching the detectors can be expressed as

$$I' = M_{11} I + M_{12} Q + M_{13} U + M_{14} V, \tag{13}$$

where M_{11}, M_{12}, M_{13}, and M_{14} are the elements of first row in the Mueller matrix **M**. For the radiance backscattered to the top of the atmosphere (TOA), $V \approx 0$. Then we can rewrite Eq. (13) as

$$I' = M_{11} I (1 + m_{12} q + m_{13} u), \tag{14}$$

where

$$m_{12} = \frac{M_{12}}{M_{11}},\ \ \mathrm{m}_{13} = \frac{M_{13}}{M_{11}},\ \ \mathrm{q} = \frac{Q}{I},\ \ \mathrm{u} = \frac{U}{I}. \tag{15}$$

Comparing Eq. (14) and Eq.(8), we get

$$h = M_{11},\ a = \left(m_{12}^2 + m_{13}^2\right)^{1/2},\ \delta = \frac{1}{2} a\tan(m_{13}, m_{12}),\ \mathrm{f} = \left(q_{12}^2 + u_{13}^2\right)^{1/2},\ \mu = \frac{1}{2} a\tan(u, q) \tag{16}$$

and

$$m_{12} = a\cos(2\delta),\ \ m_{13} = a\sin(2\delta) \tag{17}$$

B. Polarization Analysis Algorithm

In a remote sensor polarization sensitivity measurement, a linear polarized light is provided by a polarized light source. During the measurement, the polarization direction varies from 0 to 360 degrees [26]. Since the power of the light reaching the detectors of the sensor changes with polarization angle, the instrument response varies with the polarization angle. Ideally, the response fluctuates with a 2-cycle oscillation of the polarization angle as described by Eq. (7). However, in a real measurement, other orders of oscillations could also occur due to various reasons such as nonhomogeneity of the light source and multiple passes between the light source and instrument focal-plane filters [27, 28], which may provide some information about the uncertainty of the measurements [11]. The 2-cycle oscillation provides information of the instrument's polarization properties. However, the light provided by the polarization source may not be fully polarized and in such case Eq. (8) instead of Eq. (7) needs to be applied to derive the polarization factors of the instrument and the scene polarization factor has to be determined separately.

VIIRS as well as MODIS are whisk-broom scanning radiometers, This work focuses on the scanning radiometers. For a paddle broom scanning radiometer, there is a rotating two-side scan mirror which directs the light from the Earth surfaces and other targets onto the Focal Plane Assemblies (FPAs). There are multiple bands with different wavelengths and each band may have multiple detectors. The polarization phenomenon is an optical effect. Thus, the polarization properties of the instrument apparently depend on the scan angle (different optical path) of the scan mirror, the mirror side (two sides not necessarily identical), and the band (wavelength). They may also depend on the detector due to the slight different optical path among detectors of each band. For a given polarization angle α, the data may be collected in multiple scans and samples. Let $dn_{BDM\phi}(\alpha)$ be the background subtracted and scan and sample (selected) averaged response, where B is the band number, D is the detector number, M is the half-angle mirror (HAM) side, ϕ is the scan angle. The measured $dn_{BDM\phi}(\alpha)$ is fitted to a fourth-order Fourier expression [11]

$$dn_{BDM\phi}(\alpha) = c_0^{BDM\phi} + \sum_{i=1}^{4} [c_i^{BDM\phi} \cos(i\alpha) - d_i^{BDM\phi} \sin(i\alpha)], \tag{18}$$

where, and $c_i^{BDM\phi}$ and $d_i^{BDM\phi}$ are Fourier coefficients for the ith-order components. They are computed by

$$c_i^{BDM\phi} = \frac{1}{\pi} \int_{-\pi}^{\pi} dn_{BDM\phi}(\alpha) \cos(i\alpha) d\alpha, \tag{19}$$

$$d_i^{BDM\phi} = -\frac{1}{\pi} \int_{-\pi}^{\pi} dn_{BDM\phi}(\alpha) \sin(i\alpha) d\alpha. \tag{20}$$

Eq. (18) can be rewritten as

$$dn_{BDM\phi}(\alpha) = c_0^{BDM\phi} \left[1 + \sum_{i=1}^{4} a_i^{BDM\phi} \cos(i\alpha + \sigma_i^{BDM\phi}) \right], \tag{21}$$

where $a_i^{BDM\phi}$ and $\sigma_i^{BDM\phi}$ are the amplitude and phase angle of the ith-cycle oscillation, respectively. They are related to the Fourier coefficients of the same order components by

$$a_i^{BDM\phi} = \sqrt{(c_i^{BDM\phi})^2 + (d_i^{BDM\phi})^2} / c_0^{BDM\phi}, \tag{22}$$

$$\sigma_i^{BDM\phi} = \tan^{-1}(d_i^{BDM\phi}, c_i^{BDM\phi}). \tag{23}$$

As shown in Eqs. (7) and (8), the polarization effect only induces two-cycle oscillation and the polarization sensitivity of an instrument is described by a polarization factor and a phase angle. In this report, we employ $a_{BDM\phi}$ and $\delta_{BDM\phi}$ to denote the polarization factor and phase angle, respectively. In the ideal case, they are equal to the amplitude and the phase angle of the two-cycle oscillation by

$$a_{BDM\phi} = a_2^{BDM\phi} \quad \text{and} \quad \delta_{BDM\phi} = -\frac{1}{2} \sigma_2^{BDM\phi}, \tag{24}$$

and the amplitudes of all non-two-cycle oscillations are zero. The unexpected one-, three-, four-cycle, or even higher order oscillations represent the noise of light source and instrument fluctuation, which may also have contributions to the two-cycle oscillation [11]. Considering the contributions of the noise and fluctuation to the two-cycle oscillation should have some kind of relationship to the oscillations of other cycles, the amplitudes of the non-two-cycle oscillations can be used to estimate the uncertainty of the polarization factors and phase angles derived

from the measurements. If the incident light is not fully polarized, the amplitude of the two-cycle oscillation, $a_2^{BDM\phi}$, derived from Eqs. (19)-(22) is smaller than the actual polarization factor. Then the degree of the polarization of the incident light should be determined as mentioned previously and the polarization factor can be determined by taking the ratio of the amplitude of the two-cycle oscillation, $a_2^{BDM\phi}$, and the degree of the polarization of the incident light.

C. Polarization Correction to EV Reflectance and Radiance

The primary Level 1B products (also referred to as sensor data records, or SDR) of a remote sensor for a reflective solar band B are the EV radiance $L_{EV,B}$ and reflectance $\rho_{EV,B}\cos(\theta_{EV})$, where ρ_{EV} is the Earth scene bi-directional reflectance factor (BRF) and θ_{EV} is the solar zenith angle of the Earth scene. The RSB are calibrated using on board SD and SDSM. They are also calibrated using the scheduled lunar observations. Both are considered to provide non-polarized light sources for MODIS RSB calibration as mentioned previously. Thus, the L1B products are accurate provided that the EV light is non-polarized or that the polarization effect is negligible. According to Eq. (8), the actual EV radiance and reflectance can be expressed as [11]

$$L_{EV,B} = \frac{\lfloor L_{EV,B} \rfloor_{L1B}}{c_{pl}(B,D,M,\phi)} \tag{24}$$

and

$$\rho_{EV,B}\cos(\theta_{EV}) = \frac{\lfloor \rho_{EV,B}\cos(\theta_{EV}) \rfloor_{L1B}}{c_{pl}(B,D,M,\phi)}, \tag{25}$$

where

$$c_{pl}(B,D,M,\phi) = 1 + a_{BDM\phi} f \cos\lfloor 2(\mu - \delta_{BDM\phi}) \rfloor \tag{26}$$

is the polarization correction factor. The scene polarization factor f and the polarization angle μ depend on wavelength of the band and vary with geolocation and the observation geometry. The polarized scene light can also be described by a Stokes vector and the instrument polarization sensitivity be characterized by a Mueller matrix as discussed previously. Then the polarization correction factor can also be written as

$$c_{pl}(B,D,M,\phi) = 1 + m_{12}q + m_{13}\mu . \tag{27}$$

For ocean surfaces, the main contribution to the polarization of the Earth reflected sunlight comes from the Rayleigh scattering, which has been well studied and various models have been developed to describe the effect. In other words, q and u can be calculated using a Rayleigh scattering model for an ocean surface. They are scene and time dependent. m_{12} and m_{13} can be calculated from the polarization factor and phase angle using Eq. (17). It is noted that the correction approach should be based on the requirement from science and applications, i.e., different disciplines (atmosphere, land, and ocean) may have different approaches.

III. SNPP VIIRS PRELAUNCH MEASUREMENTS AND DATA ANALYSIS

SNPP VIIRS polarization sensitivity was measured on three separate occasions [18-21]. The first polarization sensitivity test (called FP-11) was performed during the testing phase at the instrument level at Raytheon's Goleta facility in the fall of 2007 using the Polarization Source Assembly (PSA) as the polarized light source [31]. Since the intensity of the light had a strong polarization direction dependence demonstrated by the large unexpected one-cycle oscillation, it was believed that the measurement uncertainty may be larger than the polarization measurement uncertainty specification [18]. The results of the first test were abandoned along with the testing equipment in a consensus choice to use a new test configuration. The second test, Special Test Request 554 (STR554), was performed in the ambient test phase at Raytheon's El Segundo facility using a large (100 cm diameter) Spherical

Integrating Source (SIS) and two 12-inch diameter Polaroid sheets to produce polarized light. The test results demonstrated that the erratic noise in the new test configuration was significantly reduced [19, 21]. However, unexpected variations across the detectors of a single band were observed. In fact, the variations were already observed in the first test, but it was believed that they were induced by the erratic noise and would be removed with new test configuration. It was also found that the scattering light had non-negligible contributions to the 2-cycle oscillation due to the rectangular shape of the SIS's aperture used in the test [21]. With the doubt about the validity of the second test results, the third VIIRS polarization sensitivity test, Engineering Test Procedure 679 (ETP679), was performed in post Thermal Vacuum (TV) phase with a same approach used in the second test except that the rectangular aperture on the SIS was replaced by a circular aperture to prevent the potential contamination of the scattering light to the polarization effect and the test covers all bands and selected scan angles [20, 21]. In this paper, we derive the polarization parameters of the SNPP VIIRS RSB using the measurements from the third polarization sensitivity test, which is the most reliable test among the three tests and is believed to provide the true polarization sensitivity of the SNPP VIIRS.

In the EPT679 test, the two Polaroid sheets BVO777 and BVONIR were used, BVO777 for shorter wavelength bands M1-M3 and BVONIR for other longer wavelength bands M4-M7 and I1-I2. There was an overlap region where both sheets worked well and could be used to check the consistency of the measurements. In the test, a blocking filter was also used to cut off the light with wavelengths longer than 600 nm. The measurements were first implemented to check the setup of the test, the performance of the two filters, and the instrument's response to the background. Then, the measurements were implemented at three different radiance levels, using the two polarizer sheets, with a blocking filter out or in, and at seven scan angles: -55^o, -45^o, -20^o, -8^o, 22^o, 45^o, 55^o for both HAM sides A and B. For each scan angle, the measurements were implemented at 25 polarization angles covering the angle from -180 to 180 degrees with a step of 15 degree. Figure 4 shows the coordinate system in which the polarization angle is defined in the test, where **z** vector is along the propagation direction, **x** vector is along the track direction or instrument flight direction, and **y** is perpendicular to the plane formed by **x** and **z** and along the direction of $\mathbf{S} \times \mathbf{X}$. When Eq. (26) or Eq. (27) is applied to correct the polarization effect in EV scene radiance or reflectance, the scene polarization angle μ or components q and $\underline{u}$ of the scene Stokes vector have to be defined in the coordinate system shown in Figure 4.

The measured data were grouped into UAIDs (unique acquisition identifiers). Every UAID either for testing the performance of the filters or measuring the polarization properties for a given scan angle contains 25 collects, each for one of the 25 selected polarization angles. Each collect in the UAID contains 128 scans and in each scan, there are 2048 (M-bands) or 4096 (I-bands) samples. Since the Rotating Telescope Assembly (RTA) was rotating during the test, the background response of the instrument was obtained from the Space View (SV) data. Of the 128 scans, 64 scans were for each HAM side. Then, we averaged the background-subtracted response over the scans of each HAM side. Since the SIS has a finite size, not all samples were fully illuminated. To determine which samples were fully illuminated by the SIS, we first found the sample which had a maximum scan-averaged response and then all samples whose response were within 4% of the maximum were selected. By averaging over these selected samples, we acquired the average background subtracted response. By applying the above approach, we obtained the background-subtracted response for each detector, band, HAM side, and polarization angle from each UAID at each selected scan angle. In the UAIDs, the instrument order was used to number the detectors of each band. Then in this section and figures shown in this section, the detectors are numbered in instrument order.

Figures 5 and 6 display the response, background subtracted digital number (dn), for band M1 HAM A obtained from UAID 3104566 and for band I2 HAM A obtained from UAID 3014568, respectively. D01, D02, …, D16 in the two figures represent detector 1, detector 2, …, detector 16 of the bands, respectively. There were two BVO777 polarizer sheets and blocking filter used in measurements when UAID 3104566 was collected. One BVO777 polarizer sheet was fixed and another polarizer sheet changed the polarization angle from -180^o to 180^o with steps of 15^o. The blocking filter was used in the measurement to block the light at longer wavelengths. For UAID 310458,

there are also two BVONIR polarizer sheets used in the measurements, one with fixed polarization angle and one with polarization direction rotating. Figures 5 and 6 demonstrate that BVO777 and BVONIR can provide fully polarized light for band M1 and I2, respectively. In fact, BVO777 can provide fully polarized light for bands M1-M3, while BVONIR can for bands M4-M7 and I1-I2.

Figures 7 and 8 show the averaged instrument responses to the polarized light for M1 HAM A and I2 HAM B. The two plots show nearly perfect two-cycle oscillations. This indicates that the impact of the non-uniformity of the light source and other noise is small. It is seen from these plots that the amplitudes and the phase angles of the oscillations are clearly detector dependent. This implies that the polarization factors are strongly detector dependent for these two bands. For other bands, they are also strongly detector dependent. This will be shown in detail in later sections.

Figures 9 and 10 show the polarization factors and phase angles for the band M1 derived from the following UAIDs: 3104581, 3104610, 310461, 3104614, and 3104628. During the measurements, the polarizer sheet BVO777 was used to provide polarized light and a blocking filter was used in four UAIDs to filter out the light with longer wavelengths (longer than 600 nm). The blocking filter was not used in one UAID (3104614) but was used in other four UAIDs. From Figures 9 and 10, it is seen that the polarization factors and phase angles derived from UAID 3104614 have observable differences from those derived from other four UAIDs. It is understandable that the blocking filter used in the test greatly reduced the contribution from the out of band relative spectral response (OOB RSR). For band M1, a relative large OOB RSR is found during prelaunch test [30]. The polarization effect depends on the spectral distribution of the incident light since the polarization effect is wavelength dependent. The OOB contribution is significantly reduced when the filter is applied to filter out the light with wavelength longer than 600 nm and then the polarization parameters measured with and without are different as displayed in Figs. 9 and 10. The OOB RSR contribution is about 2.85% at launch and has reduced to 2.26% after three years on-orbit due to the large degradation of the rotating telescope assembly (RTA) in near infrared spectral range [31]. If the radiance of incident light is evenly distributed over wavelength, the contribution of the OOB RSR to the polarization effect is estimated to be less than 0.1% according to the percentage of the OOB RSR. In fact, the solar radiance has larger distribution in the visible spectral range than in near infrared range. Then the effect of OOB RSR on the polarization effect on-orbit is even smaller and becomes negligible considering the uncertainty specification of the RSR which is 2% and tolerant for ocean color EDR which has a stringent requirement of ~0.2% for the accuracy of the calibration. The OOB RSR impact is magnified in the prelaunch measurements as shown in Figs. 9 and 10 due to the much larger distribution of the radiance in the near infrared spectral range than in the visible range around 412 nm (the center wavelength of band M1). Thus, in this analysis only the polarization parameters derived from the measurements with the filter applied are further averaged to obtain those for band M1.

Figures 11 and 12 show the band I1 HAM A polarization factors and phase angles derived from the following UAIDs: 3104581-3104583, 3104612, 3104614, 3104617, 3104618, and 3104628-3104630. During the measurements, the polarizer sheet BVONIR was used to provide the polarized light. Similar to the band M1, there was a blocking filter which could be used to reduce the incident light intensity. As mentioned above, the filter mainly reduces the radiance level of the light at longer wavelengths. From Figures 11 and 12, it is seen that the polarization factors and phase angles derived from the data with and without the blocking filter are quite different. Since the blocking filter reduces the incident radiance for the band I1 and relatively increases noise due to the crosstalk from short wavelength bands, the polarization parameters derived from the UAIDs with the blocking filter used during the test are less reliable. Only those derived from the UAIDs without the blocking filter inserted during the measurements should be used to derive the polarization parameters for the band I1.

The polarizer sheet BVO777 is designed to provide polarized light for visible light, while polarizer sheet BVONIR should provide well polarized light for near-infrared (NIR) light. In principle, one can always derive the polarization parameters for SNPP VIIRS visible bands from the data using BVONIR to provide polarized light and

for NIR bands from the data using BVO777 as polarized light provider. However, in practice the instrument responses of the visible bands are too small in the UAIDs, which were collected when BVONIR was used to provide polarized light. In contrast, when BVO777 was used as polarized provider during the test, there were cases in which the instrument responses of the band M4 are saturated while those of the NIR bands are too small, due to the use of the blocking filter, to be used to derive the polarization parameters. But in other cases, the data measured with BVO777 as polarized light provider can be used to derive the polarization parameters for bands M4-M7 and I1-I2. The polarization parameters derived from these data are very consistent with those derived from the UAIDs obtained using BVONIR as polarized light provider for all NIR bands except bands M7 and I2. For bands M7 and I2, the light provided by BVO777 is not fully polarized and the derived polarization factors are smaller. The degree of polarization for the light provided by BVO777 for bands M7 and I2 can be derived from UAID 3104567, where two BVO777 polarizer sheets were used in the test, one fixed polarization angle while the other with polarization angle varied from -180^{o} to 180^{o}. Then from the data, the degree of the polarization of the polarizer sheets can be determined, which is the factor should be used to correct the derived polarization parameters. Analysis shows that a correction factor of 0.5930 and 0.5966 should be applied for the band M7 and I2, respectively, to the polarization factors derived from the UAIDs measured using BVO777 as polarized light provider. With the correction, the polarization parameters derived from the data obtained with BVO777 agree well with those obtained from the data measured with BVONIR for bands M7 and I2.

Figures 13 and 14 show the polarization factors derived from the UAIDs obtained with BVO777 for the band M1 and from those measured with BVONIR for the band M4, respectively. For each band, there were several measurements and the derived polarization factors from different UAIDs agree within ~0.1%. Considering the requirement for the uncertainty of the measurements is 0.5%, the measurements have a very high repeatability. By averaging the polarization parameters shown in Figures 13 and 14, we can obtain the polarization factors for bands M1 and M4. We can obtain the polarization parameters for other bands in the same way. For bands M1-M3, the polarization parameters are derived from the UAIDs obtained with BVO777 as polarized light provider and for bands M4-M7 and I1-I2, the polarization parameters are derived from the data measured with BVONIR. Even though the polarization parameters for the NIR bands can also be derived from some of the UAIDs obtained with BVO777, the data are not used in this report for the derivation of polarization parameters of the NIR bands.

The one-cycle oscillation amplitudes for all the data used to derive polarization parameters are derived and analyzed. They are all smaller than 0.2%. The three- and four-cycle oscillation amplitudes are also derived and they are even smaller as expected. Thus, the uncertainty of the non-uniformity of light source or other noise which induced one-cycle oscillation in the instrument's response should be less than 0.2%. As demonstrated above, the measurements have a very high repeatability. The uncertainty due to repeatability of the measurements used in this analysis to derive the polarization parameters is smaller than 0.15% for all VisNIR bands. The uncertainty of the measurements due to other noise is estimated to be less than 0.3%. From the analysis, the total uncertainty of the derived polarization factors should be less than 0.5%, which is specification for the uncertainty of the instrument's polarization sensitivity characterization.

IV. POLARIZATION FACTORS AND PAHSE ANGLES

The polarization effect may be corrected by using either Eq. (26) or Eq. (27). The polarization factors and phase angles are derived from the EPT679 test for all VisNIR bands at the seven selected scan angles. In this section, we will show the derived polarization factors and phase angles and discuss the results. Since in most cases, the Stokes vector is used to describe the polarization of the sunlight reflected from the earth surface. Thus, it is more convenient to use Eq. (27) to correct the polarization effect. In these cases, the polarization factors and phase angles need to be converted to normalized Mueller matrix elements, m12 and m13, by using Eq. (17). We will also show the obtained m12 and m13 in this section. Since the production order, which is just opposite to the instrument order,

is applied in the SNPP VIIRS SDR and EDR, we use the production order for the detectors of each band in this section (also all figures shown in this section).

Figures 15 and 16 show the polarization factors for the band M1 HAM A and B, respectively. From these two figures, it is evident that for the band M1, the difference between HAM A and B for the polarization sensitivity is small. As seen in previous tests, the polarization factors of the band M1 are strongly detector dependent as well as scan angle dependent. Figures 17 and 18 show the polarization phase angles. Similar to the polarization factors, the polarization phase angles of the band M1 have strong detector and scan angle dependence, but are hardly HAM dependent. Figures 19 and 20 display the polarization factors for the band M2 and M3 HAM A, respectively. As with the band M1, the factors for both bands M2 and M3 are strongly detector and scan angle dependent. From Figures 15-16 and 19-20, it can also be seen that the polarization factors of different detectors in a given band cross and the cross point moves to smaller scan angle with increasing wavelength. From these plots, it is seen that all the four bands satisfy the polarization sensitivity specification, which is 3% for bands M1, I2, and M7 and 2.5% for all other bands.

Figures 21 and 22 display the polarization factors for the band I1 (640 nm) HAM A and B, respectively. As with bands M1-M3, they are detector dependent as well as scan angle dependent. But different from those for bands M1-M3, they are also strongly HAM dependent. It can also be seen that the detector dependence of the polarization factors of the band I1 is quite different from the dependence of those of bands M1-M3. For example, detector 1 of the band I1 has the largest polarization factor at small scan angle, while detector 16 in bands M1-M3 has the largest polarization factor at same scan angle region. The HAM dependence of the polarization factors is also observed for bands M4 (555 nm) and M5 (670 nm). It only happens for bands with wavelengths around 600 nm. This phenomenon was also observed in the polarization factors derived from the previous tests.

Figures 23 and 24 show the detector-averaged polarization factors for HAM A and B, respectively. Band M1 has the largest polarization factor at all scan angles. The polarization factors of the band M1 at all scan angles and for both HAM A and B are smaller than 2.5%. Thus, the polarization factors of VIIRS F1 band M1 are seen again to be within the specification. In Figure 16, it is shown that the polarization factor of the band M1 detector 16 HAM B at -55^{o} is larger than 3%. However, since the specification does not apply to -55^{o}, the band still passes the specification. For all other bands, the polarization factors at all scan angles and HAM are less than 2%, and thus are within the polarization sensitivity specifications listed in Table 1 for these bands. For completeness, the polarization factors and phase angles for all VisNIR bands, detectors, HAM sides, and the scan angles are shown in Figures 25 and 26, respectively. From these two figures, the dependence of the polarization sensitivity on the band, detector, HAM side, and scan angle, especially HAM side, can be clearly seen.

Compared to both Terra and Aqua MODIS [11], SNPP VIIRS is much less sensitive to the polarization of the incident light. Furthermore, the SNPP VIIRS polarization factors become smaller at large scan angle while those for the two MODIS instruments increase with the scan angle for the short wavelength bands, which have larger polarization effect. The angle of incidence (AOI) on the scan mirror of a MODIS instrument has a simple linear relationship with the scan angle while that on the HAM of SNPP VIIRS has a little more complex relationship with the scan angle. For the EV sector, the AOI increases with the scan angle in a MODIS instrument while it decreases with the scan angle in a VIIRS instrument. Thus, the polarization factors of the short-wavelength bands increase with the AOI in both MODIS and VIIRS instruments. This is understandable since the scan mirror in MODIS and the HAM in VIIRS determine the variations of the polarization factors with the scan angles of the two instruments. Since the degree of the polarization of the incident light is small at small scan angle while large at large scan angle, the aforementioned features of the polarization factors of the three instruments magnify the polarization effect for the VisNIR bands of the two MODIS while compress the effect for those of SNPP VIIRS. For both MODIS instruments, the polarization factors increase to about 6% at large scan angle. For SNPP VIIRS, they decrease to about 1% as shown in Figs. 15 and 16 at large scan angle. This indicates that the actual polarization effects in the

EV radiance or reflectance of the two MODIS instruments are about 6 times larger than in that of SNPP VIIRS. In addition, the polarization sensitivity may change on-orbit. In fact, the polarization sensitivity of Terra MODIS has changed dramatically after passed its designed six-year life time after on-orbit [32]. For SNPP VIIRS, the on-orbit polarization sensitivity change should be smaller since its HAM degrades much slower due to being installed inside of the instrument. Further discussion about the on-orbit change of the polarization sensitivity is beyond the scope of this paper.

Figures 27 and 28 show m12 and m13 for the SNPP VIIRS band M1 HAM A. Symbols are the measured data for the selected seven scan angles, which are converted from the polarization factors and phase angles shown above using Eq. (17). In a real application, the polarization parameters are required for each of pixels along the scan. There are several thousand pixels along the scan while the polarization sensitivity measurements were only implemented at seven selected scan angles. To get the polarization parameters for any pixel or any scan angle in the EV sector, smooth functions can be used to fit the measured parameters and then the functions can be used to provide the polarization parameters for every pixel. For SNPP VIIRS, quadratic forms of scan angle are employed to fit m12 and m13. The solid lines in Figures 27 and 28 are the fitted functions, which are used in real application to correct the polarization effect in SNPP VIIRS SDR and EDR. It is seen in Figures 27 and 28 that the measured m12 and m13 vary with the scan angle smoothly and the fitted quadratic forms describe the parameters very well. For completeness, the m12 and m13 for all SNPP VIIRS VisNIR bands are displayed in Figures 29 and 30. As expected, they are strongly band, detector and scan angle dependent. For a few bands with wavelengths around 600 nm, they are also HAM side dependent.

The polarization parameters we derived in this analysis have been applied to correct the polarization effect in SNPP VIIRS SDR and then in EDR such as ocean color EDR. The ocean color differences between east and west in one scan are significantly reduced and the striping in ocean color images due to the detector differences is reduced as well. The detail analysis of the SDR and EDR improvements by applying the polarization correction using the polarization parameters derived in this analysis will be reported elsewhere.

V. SUMMARY

The pre-launch polarization sensitivity measurements of SNPP VIIRS are analyzed. Polarization factors and phase angles are derived for the visible and NIR bands. The derived polarization parameters are band, scan angle or AOI, and detector dependent. They are also mirror side dependent for bands I1, M4, and M5. Band M1 has largest polarization factor, which is about 3%, and the polarization factors become smaller with the increase of the wavelength of the bands. The non-uniformity of the light source used in this test is small and the incident light is either well polarized or correctable for its non-perfect polarization. In this analysis, only the data measured with well polarized light are used. It is shown that the measurements have a very high repeatability. The derived polarization factors satisfy the specification for both their values and the uncertainty of the measurements for all bands.

ACKNOWLEDGEMENTS

The current work is supported by the Joint Polar Satellite System (JPSS) funding. The sensor test data used in this document was provided by the Raytheon El Segundo testing team. Approaches for data acquisition and data reduction, as well as data extraction tools were provided by the Raytheon El Segundo. However, tools and software used in the processing of the test data, and illustrating the results have been developed by the authors with funding support from NOAA and NASA. The views, opinions, and findings contained in this paper are those of the authors and should not be construed as an official NOAA, NASA or U.S. Government position, policy, or decision.

REFERENCES

1. Cao, C.; Deluccia, F.; Xiong, X.; Wolfe, R.; Weng, F. Early on-orbit performance of the Visible Infrared Imaging Radiometer Suite (VIIRS) onboard the Suomi National Polar-orbiting Partnership (S-NPP) satellite, *IEEE Trans. Geosci. Remote Sens.*, 2014, 52, 1142–1156, 2014.
2. Xiong, X.; Butler, J.; Chiang, K.; Efremova, B.; Fulbright, J.; Lei, N.; McIntire, J.; Oudrari, H.; Sun, J.; Wang, Z.; and Wu, A. VIIRS on-orbit calibration methodology and performance, *J. Geophys. Res. Atmos.*, 119, 5065–5078, 2014.
3. Lei, N.; Wang, Z.; Fulbright, J.; Lee, S.; McIntire, J.; Chiang, K.; Xiong, X. Initial on-orbit radiometric calibration of the Suomi NPP VIIRS reflective solar bands, *Proc. SPIE*, 8510, 851018, 2012.
4. Cardema, J. C.; Rausch, K.; Lei, N.; Moyer, D. I.; DeLuccia, F. Operational calibration of VIIRS reflective solar band sensor data records, *Proc. SPIE*, 8510, 851019, 2012.
5. Sun J.; M. Wang, M. On-orbit calibration of the Visible Infrared Imaging Radiometer Suite reflective solar bands and its challenges using a solar diffuser, *Applied Optics*, 54, 7210-7223, 2015.
6. Hass, E.; Moyer, D.; DeLuccia, F.; Rausch, K.; Fulbright, J. VIIRS solar diffuser bidirectional reflectance distribution function (BRDF) degradation factor operational trending and update, *Proc. SPIE*, 8510, 851016, 2012.
7. Fulbright, J.; Lei, N.; K. Chiang, K.; Xiong, X. Characterization and performance of the Suomi-NPP VIIRS solar diffuser stability monitor, *Proc. SPIE*, 8510, 851015, 2014.
8. Sun, J.; Wang, M. Visible infrared image radiometer suite solar diffuser calibration and its challenges using solar diffuser stability monitor, *Appl. Opt.*, 36, 8571-8584, 2014.
9. Sun, J.; Xiong, X.; Butler, J. NPP VIIRS on-orbit calibration and characterization using the Moon, *Proc. SPIE*, 8510, 85101I, 2012.
10. Xiong, X.; Sun, J.; Fulbright, J.; Z. Wang; J. Butler, Lunar Calibration and Performance for S-NPP VIIRS Reflective Solar Bands, *IEEE Trans. Geosci. Remote Sensing.*, 54, 1052-1061, 2016.
11. Sun, J.; X. Xiong, "MODIS polarization sensitivity analysis", *IEEE Trans. Geosci. Remote Sens.*, 45, 2875-2885, 2007.
12. G. W. Kattawar, G. N. Plass, and J. A. Guinn, "Monte Carlo calculations of the polarization of radiation in the Earth's atmosphere–ocean system," *J. Phys. Oceanogr.*, vol. 3, no. 4, pp. 353–372, Oct. 1973.
13. A. Ivanoff, "Polarization measurements in the sea," in *Optical Aspects of Oceanography*, N. G. Jerlov and E. S. Nielsen, Eds. London, U.K.: Academic, 1974, pp. 151–175.
14. R. C. Levy, L. A. Remer, and Y. J. Kaufman, Effects of neglecting polarization on the MODIS aerosol retrieval over land, *IEEE Trans. Geosci. Remote Sensing*, **42**, 2576-2583, 2004.
15. G. Meister, E. J. Kwiatkowska, B. A. Franz, F. S. Patt, G. C. Feldman, and C. R. McClain, Moderate-resolution image spectroradiometer ocean color polarization correction, *Applied Optics*, **44**, 5524-5535, 2005.
16. Raytheon SBRS, Sensor Specification for Visible/Infrared Imager Radiometer Suite (VIIRS), PS154640-101B, February 2004.
17. Oudrari, H.; McIntire, J.; Xiong, X.; Butler, J.; Lee, S.; Lei, N.; Schwarting, T.; Sun, J. Prelaunch Radiometric Characterization and Calibration of the S-NPP VIIRS Sensor, IEEE Trans. Geosci. Remote Sens., 53, 2195-2210, 2015.
18. J. Sun**,** VIIRS FU1 Polarization-Sensitivity FP-11 Test Data Analysis, NICST_MEMO_08_009, March 4, 2008.
19. J. Sun, VIIRS FU1 Polarization-Sensitivity STR-545 Test Data Analysis, NICST_MEMO_08_023, June 24, 2008.
20. J. Sun, FU1 VIIRS Polarization Insensitivity for VisNIR Bands: ETP-679 data analysis and results, NICST_report_09_124, September 30, 2009.
21. E. Waluschka, "VIIRS polarization testing", Proc. SPIE, 7452, 745209 (2009).
22. M. Born and E. Wolf, Principles of Optics, 7th edition, Cambridge University, 1999, ISBN 0-521-64222-1.

23. Waluschka,E., "Polarization Ray Trace", *Opt. Eng.*,Vol 28,Number 2, 86-89 (1989)
24. S. Huard, Polarization of Light, John Wiley & Sons, Chichester, 1997.
25. Gordon, H. R., T. Du, and T. Zhang, "Atmospheric correction of ocean color sensors: analysis of the effects of residual instrument polarization sensitivity", *Appl. Opt.*, **36**, 6938-6948 (1997).
26. M. Pavlov, Polarization Insensitivity, Test Procedure for (ALPC-08), Santa Barbara Research Center, March 24, 1996.
27. Young, E. Knight, and C. Merrow, MODIS polarization performance and anomalous four-cycle polarization phenomenon, Proc. SPIE Vol. 3439, 247-256, 1998.
28. E. Waluschka, MODIS Polarization Measurements and Simulation and the 4θ Effect, Proc. SPIE Vol. 3121, 278-287, 1997.
29. Raytheon SBRS, Polarization Insensitivity (FP-11) Test Procedure for VIIRS, TP154640-261, April 2001.
30. C. Moeller, J. McIntire, T. Schwarting, D. Moyer, and J. Costa, "Suomi NPP VIIRS spectral characterization: understanding multiple RSR releases," *Proc. SPIE* 8510, 85101S (2012)
31. J. Sun, M. Wang, "Visible infrared image radiometer suite solar diffuser calibration and its challenges using solar diffuser stability monitor," *Appl. Opt.*, 36, 8571-8584, 2014.
32. Kwiatkowska, E.J., B.A. Franz, G. Meister, C. McClain, and X. Xiong, Cross-calibration of ocean-color bands from Moderate Resolution Imaging Spectroradiometer on Terra platform, Appl. Opt., 47, 6796-6810, 2008.

Table 1. VIIRS polarization sensitivity specification.

Band	I1	I2	I3	M1	M2	M3	M4	M5	M6	M7	M8	M9	M10	M11
Wavelength (nm)	640	862	1610	410	443	486	551	671	745	862	1238	1378	1610	2250
Specification	2.5%	3.0%	NA	3.0%	2.5%	2.5%	2.5%	2.5%	2.5%	3.0%	NA	NA	NA	NA
CW: Center Wavelength														

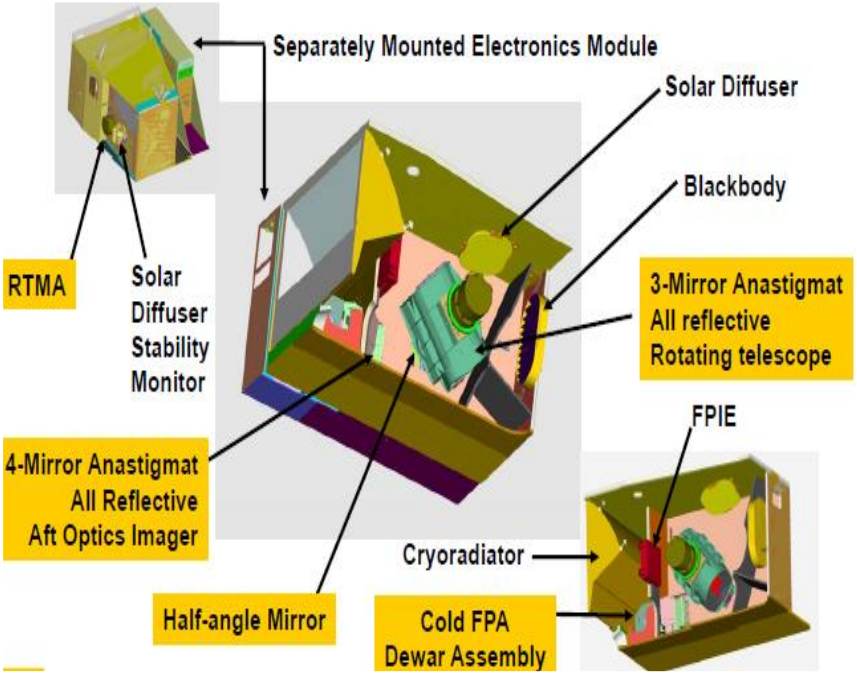

Figure 1. VIIRS instrument and its on-board calibrators.

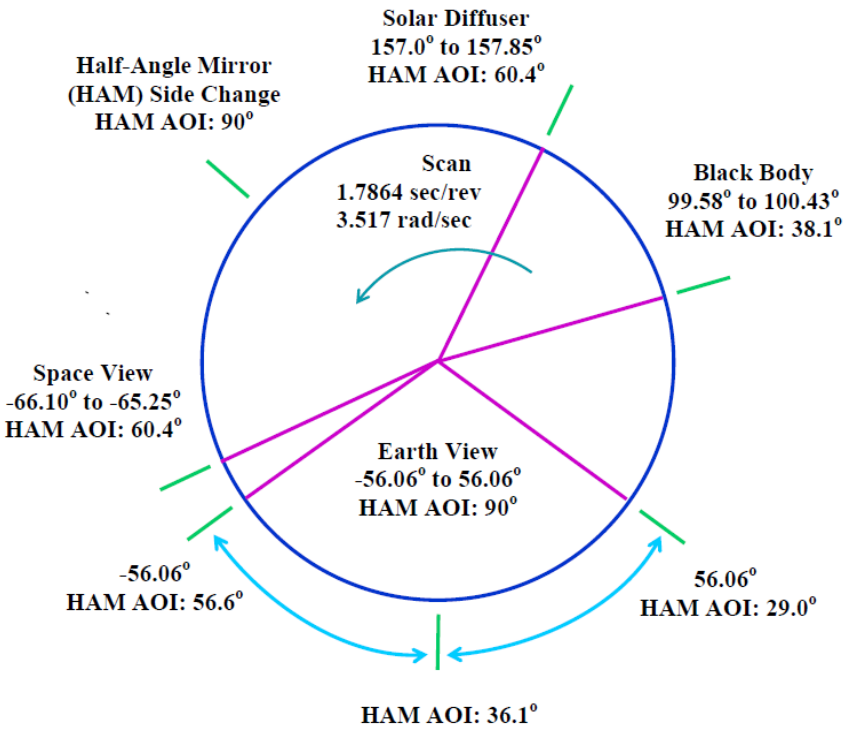

Figure 2. Scan angles of VIIRS view sectors and their corresponding AOIs on the HAM.

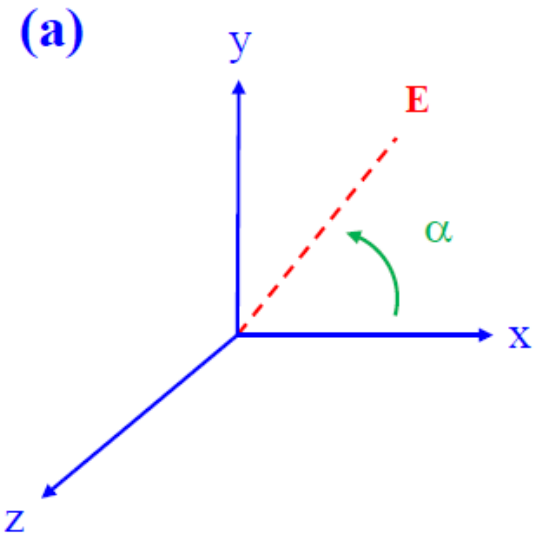

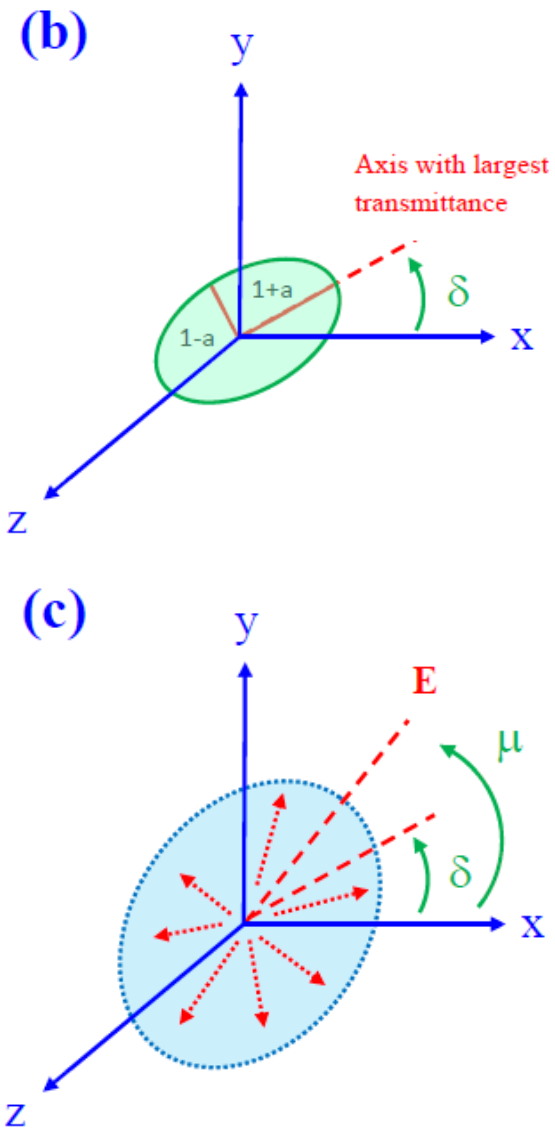

Figure 3. Definition of the polarization angle: (a) Linear polarized light; (b) Partially polarized light.

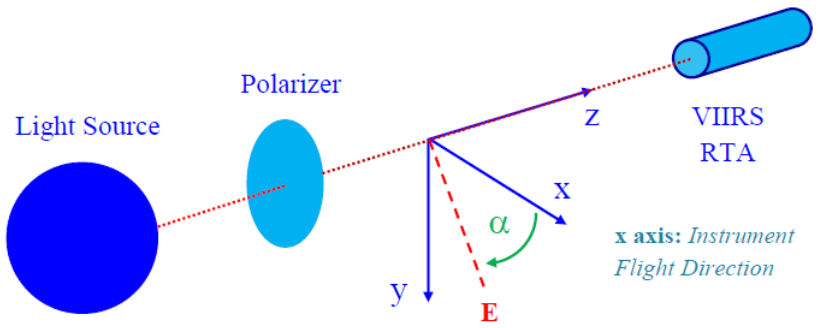

Figure 4. Definition of the polarization angle in the SNPP VIIRS prelaunch polarization sensitivity measurements.

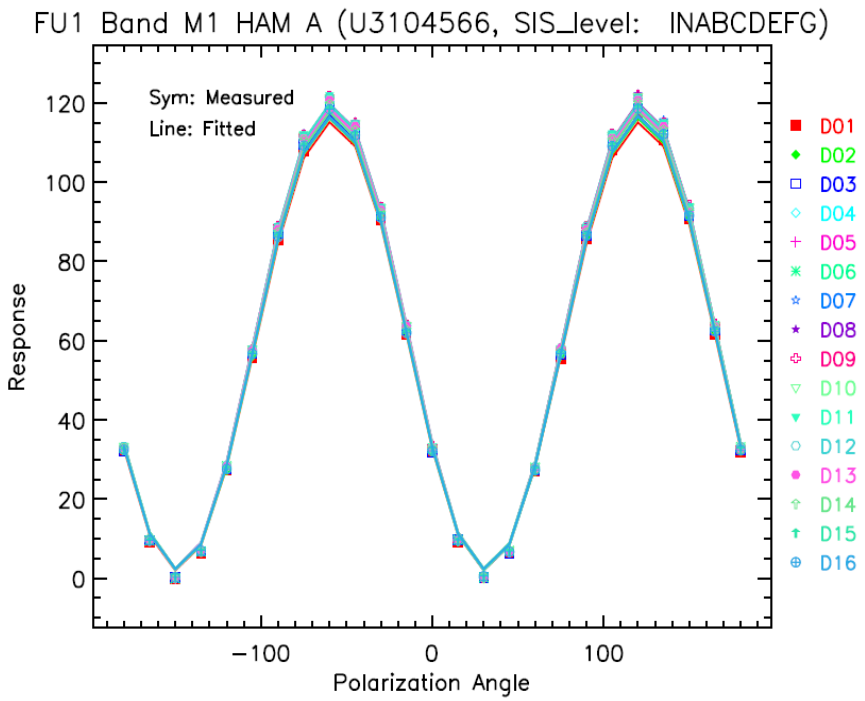

Figure 5. The responses of SNPP VIIRS (FU1) band M1 to the incident light produced by a fixed BVO777 polarizer sheet and rotating BVO777 polarizer sheet. D01, D02, …, D16 represent detector 1, detector 2, …, detector 16, respectively.

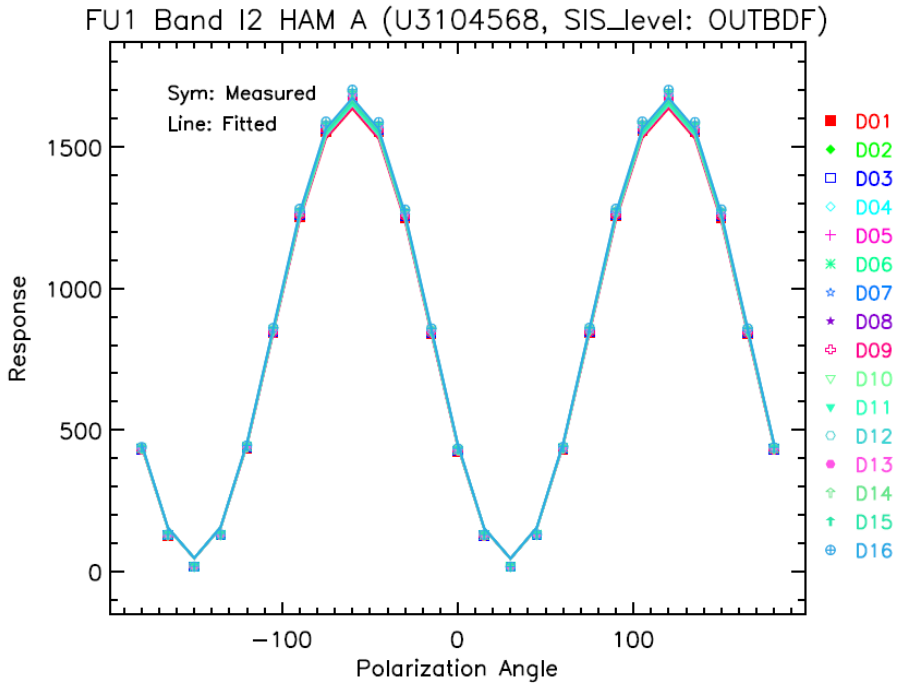

Figure 6. The responses of SNPP VIIRS (FU1) band I2 to the incident light produced by a fixed BVONIR polarizer sheet and rotating BVONIR polarizer sheet. D01, D02, …, D16 represent detector 1, detector 2, …, detector 16, respectively.

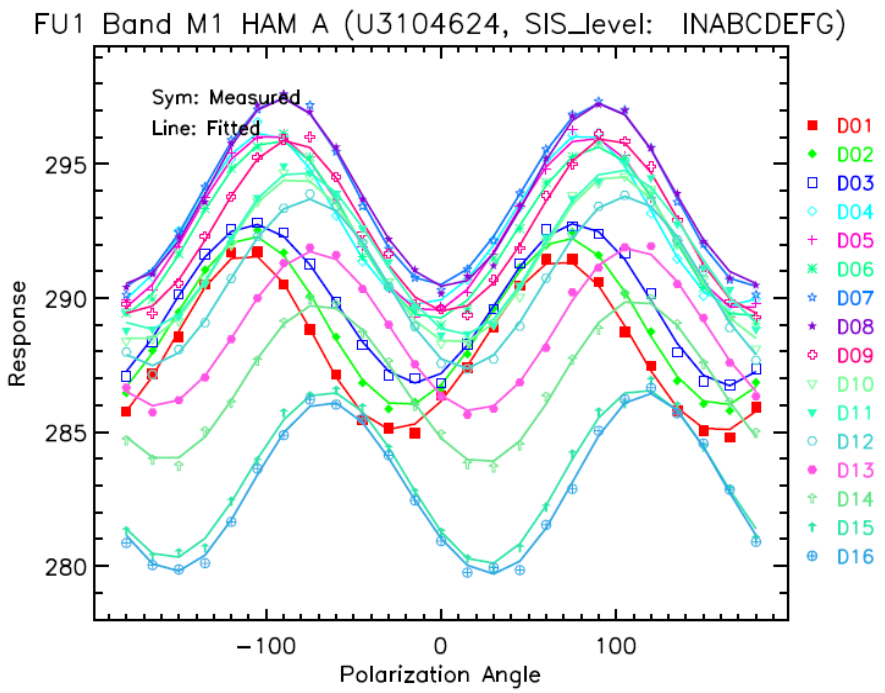

Figure 7. The responses of SNPP VIIRS (FU1) band M1 to the polarized light provided by the SIS with a polarizing sheet (UAID 3012477).

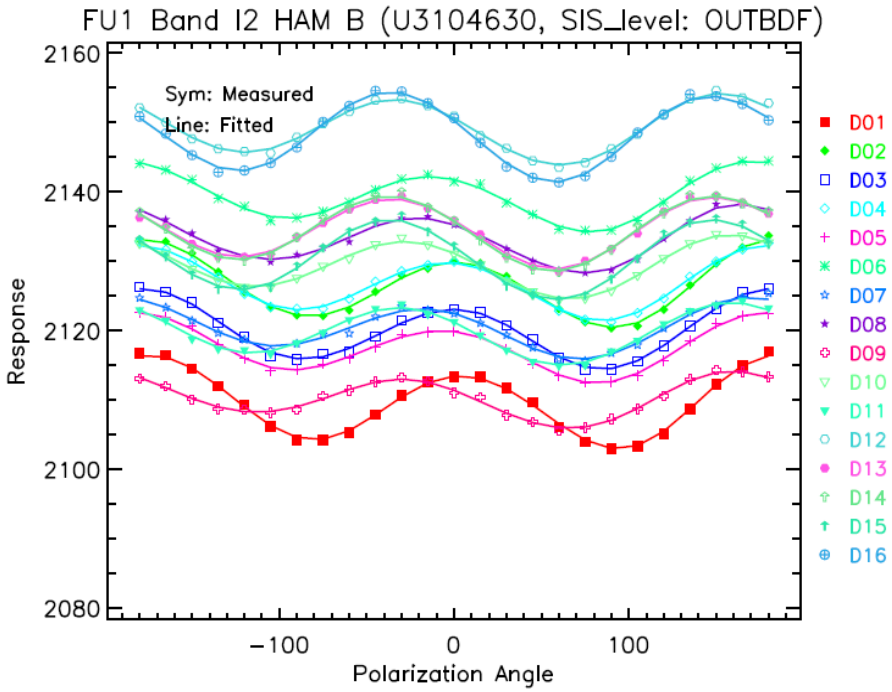

Figure 8. The responses of SNPP VIIRS (FU1) band I2 to the polarized light provided by the SIS with a polarizing sheet (UAID 3012477).

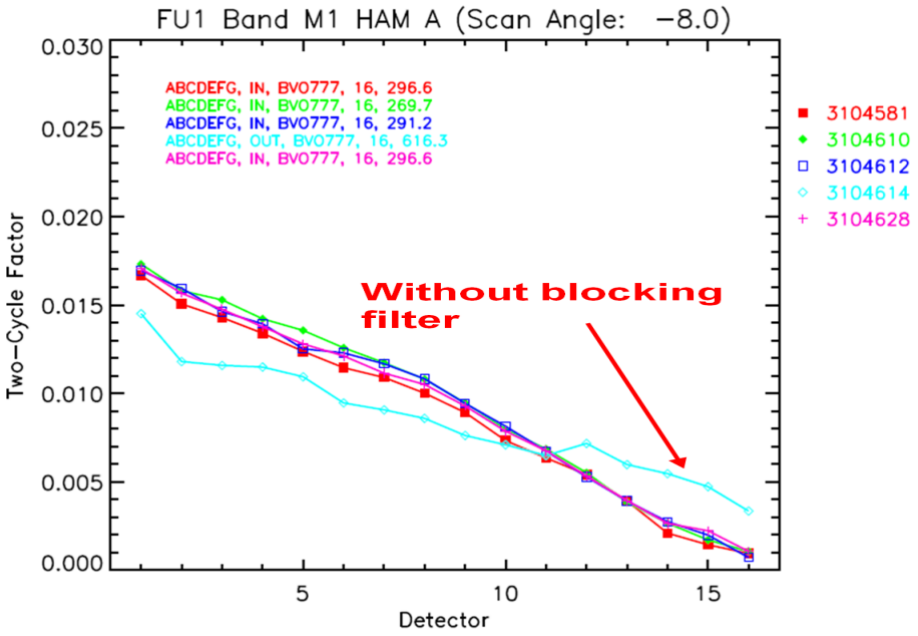

Figure 9. SNPP VIIRS (FU1) band M1 polarization factor derived from different UAIDs using polarizer sheet BVO777.

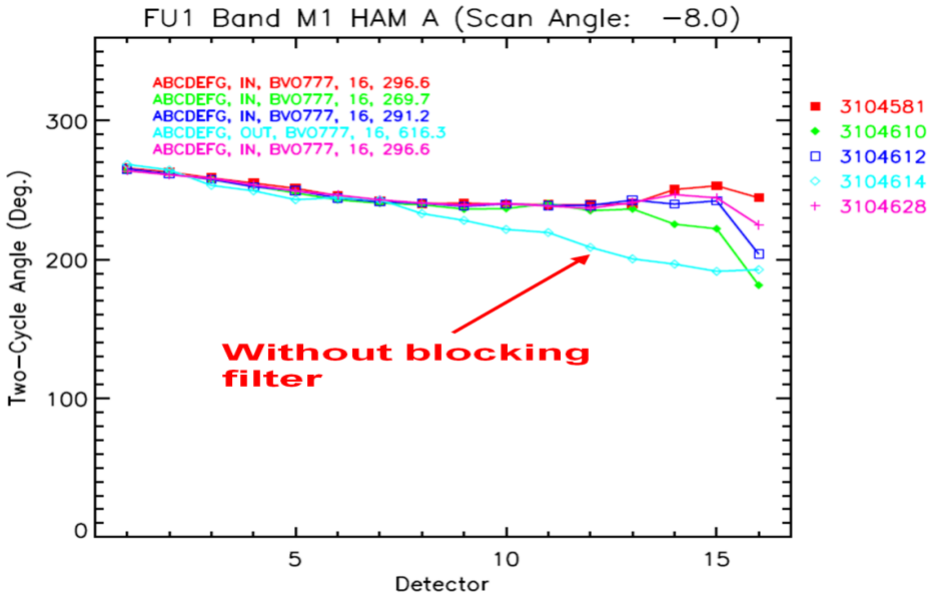

Figure 10. SNPP VIIRS (FU1) band M1 polarization phase angle derived from different UAIDs using polarizer sheet BVO777

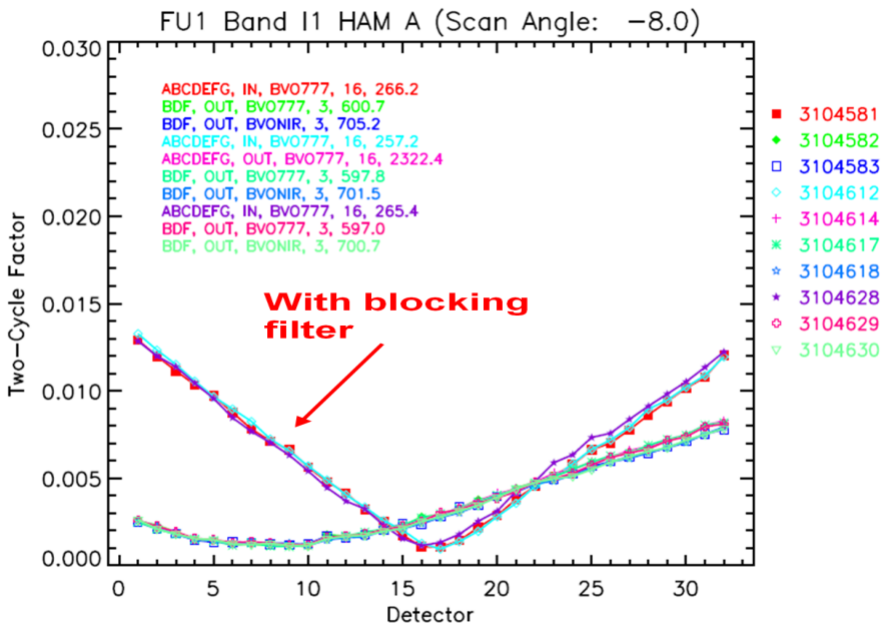

Figure 11. SNPP VIIRS (FU1) band I1 polarization factor derived from different UAIDs using polarizer sheet BVONIR.

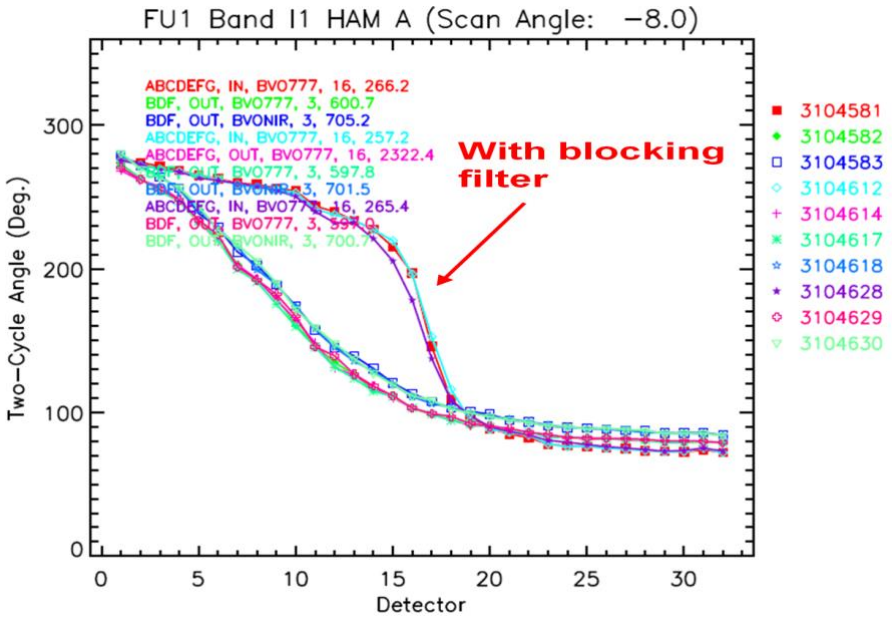

Figure 12. SNPP VIIRS (FU1) band I 1 polarization phase angle derived from different UAIDs using polarizer sheet BVONIR.

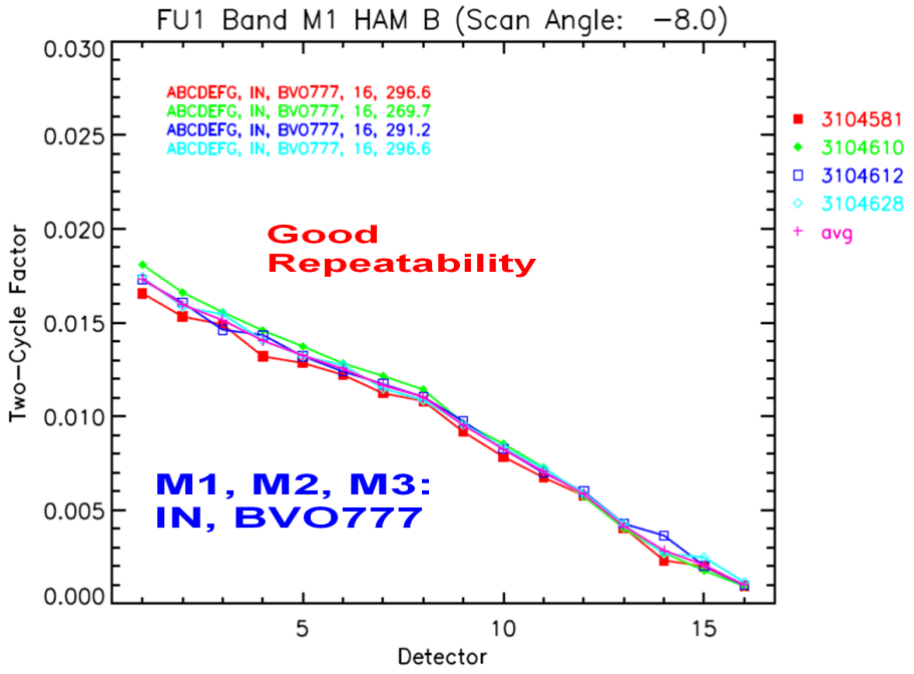

Figure 13. SNPP VIIRS (FU1) band M1 HAM B polarization factors derived from the UAIDs with BVO777 as polarized light provider.

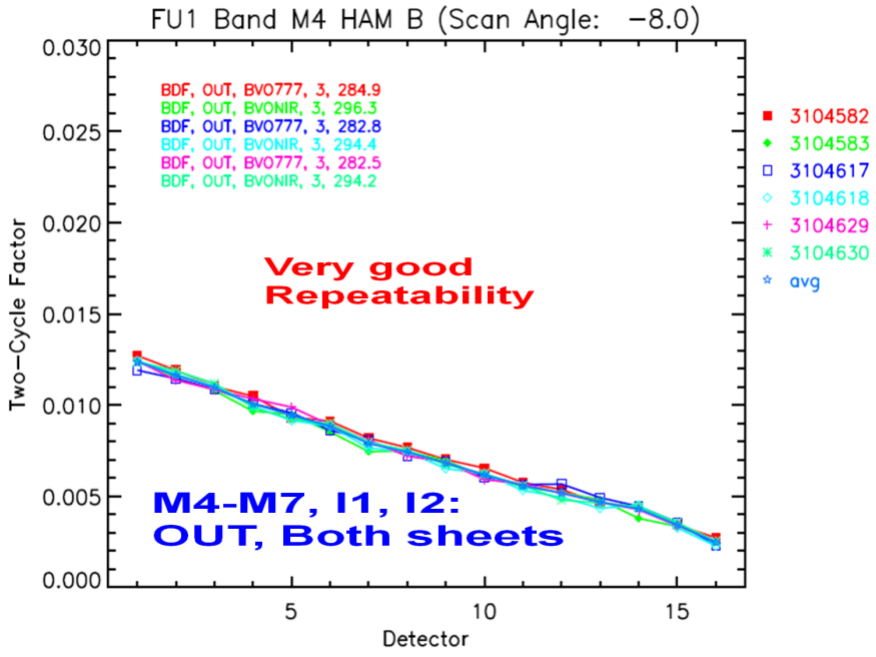

Figure 14. SNPP VIIRS (FU1) band M4 HAM B polarization factors derived from the UAIDs with BVONIR as polarized light provider.

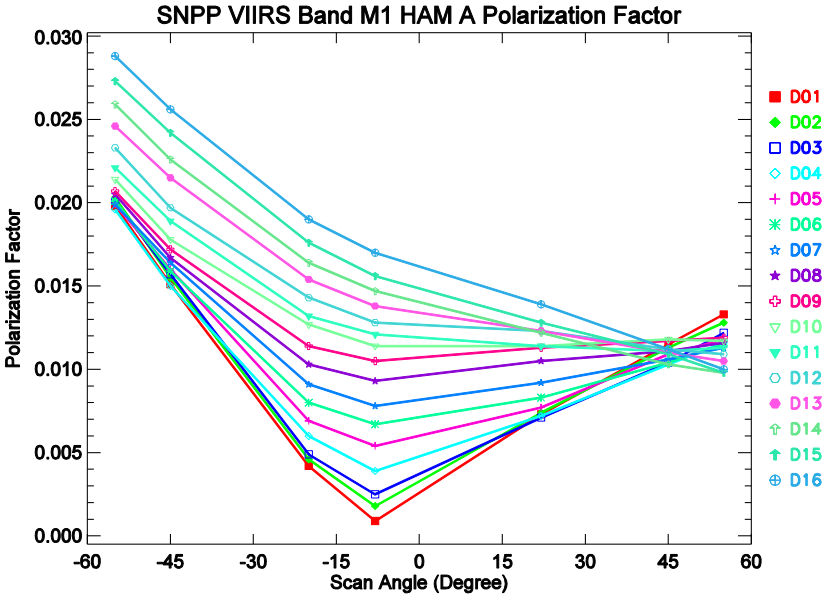

Figure 15. Polarization factors for SNPP VIIRS (FU1) band M1 HAM A.

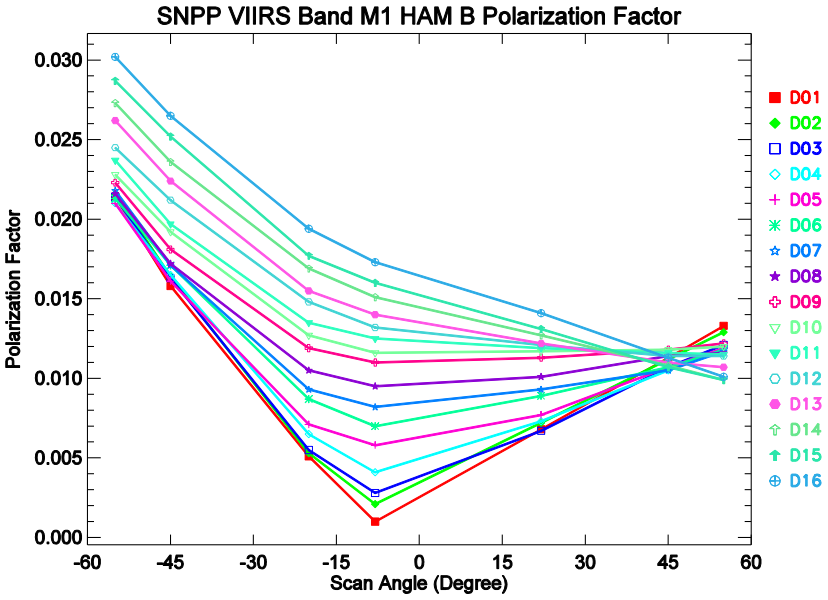

Figure 16. Polarization factors for SNPP VIIRS (FU1) band M1 HAM B.

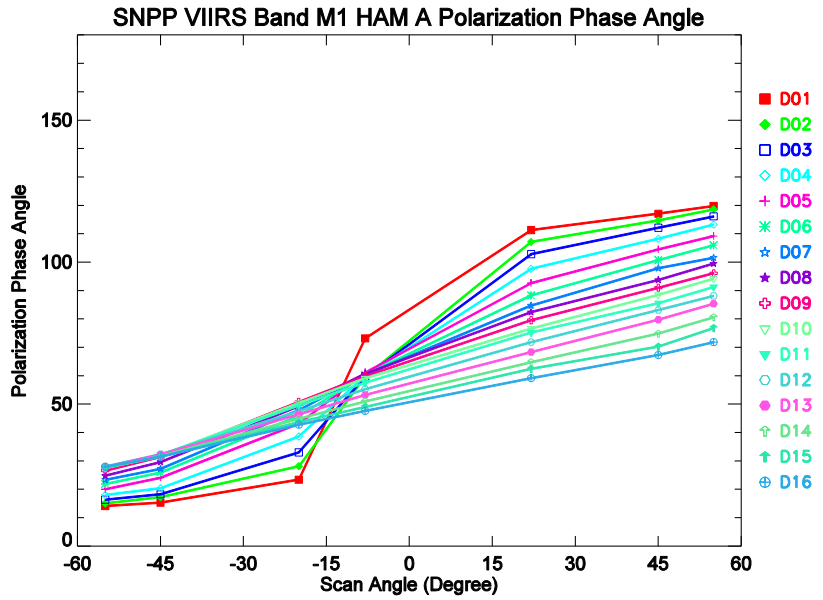

Figure 17. Polarization phase angles for SNPP VIIRS (FU1) band M1 HAM A.

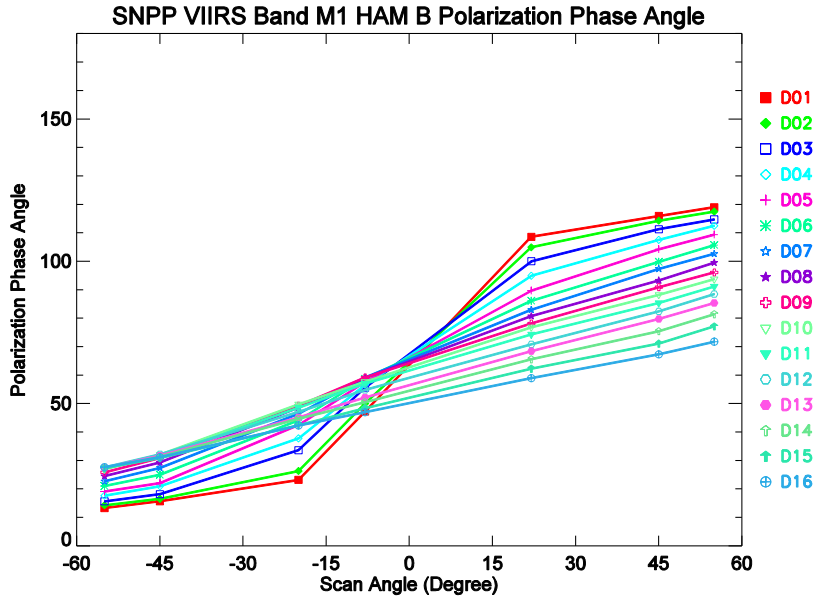

Figure 18. Polarization phase angles for SNPP VIIRS (FU1) band M1 HAM B.

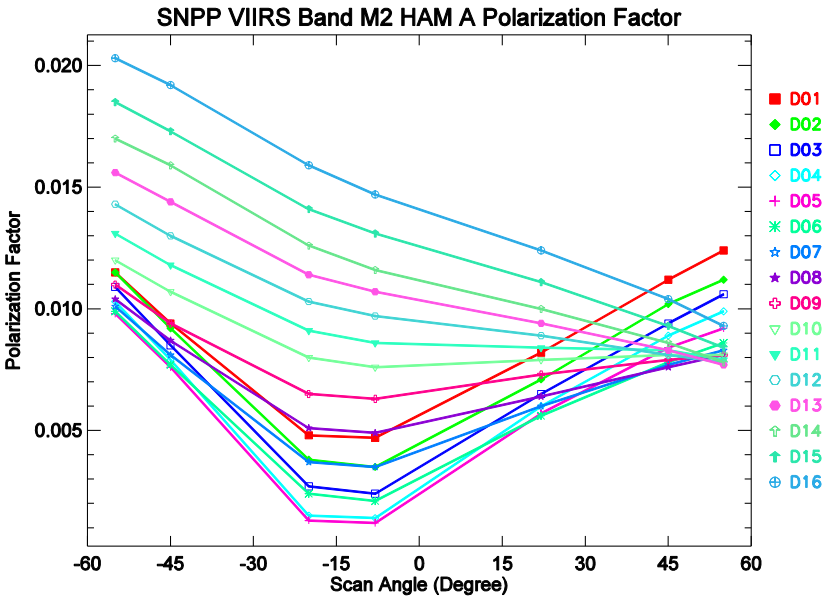

Figure 19. Polarization factors for SNNP VIIRS (FU1) band M2 HAM A.

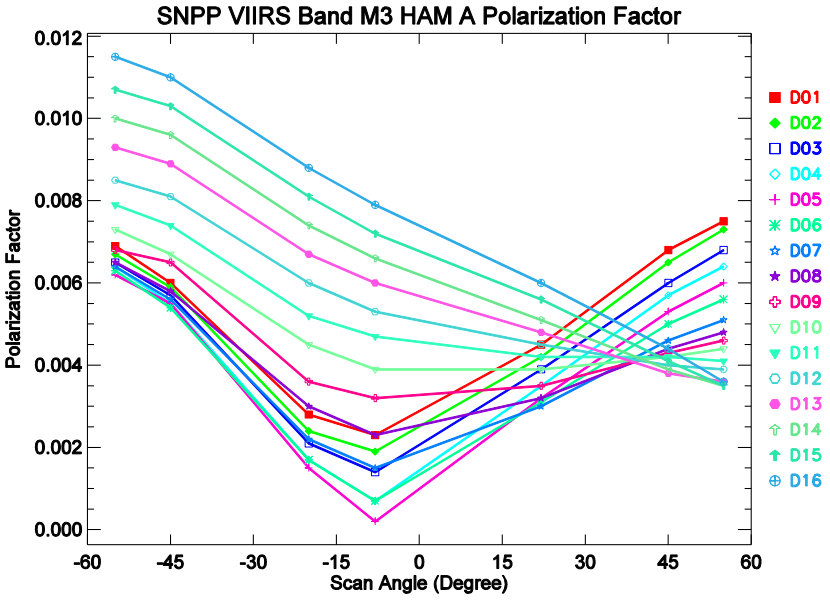

Figure 20. Polarization factors for SNPP VIIRS (FU1) band M3 HAM A.

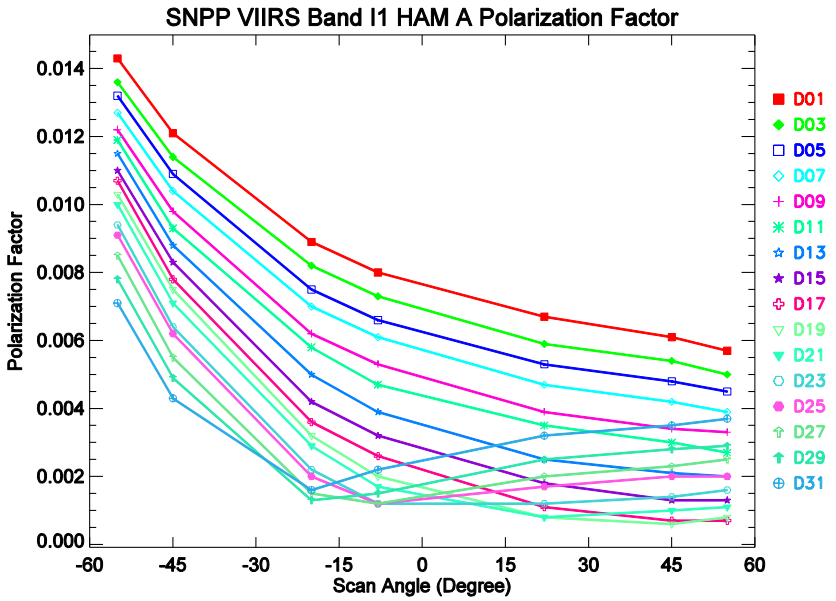

Figure 19. Polarization factors for band I1 HAM A.

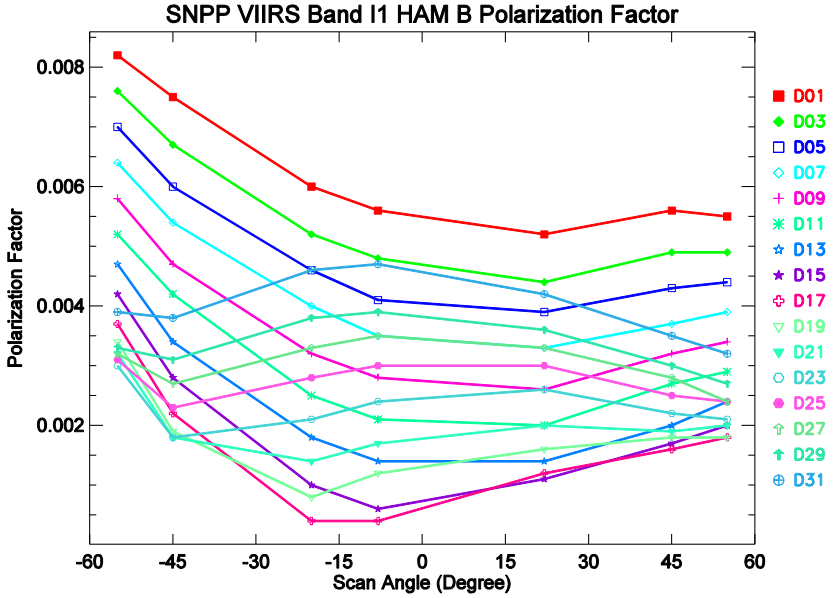

Figure 22. Polarization factors for SNPP VIIRS (FU1) band I1 HAM B.

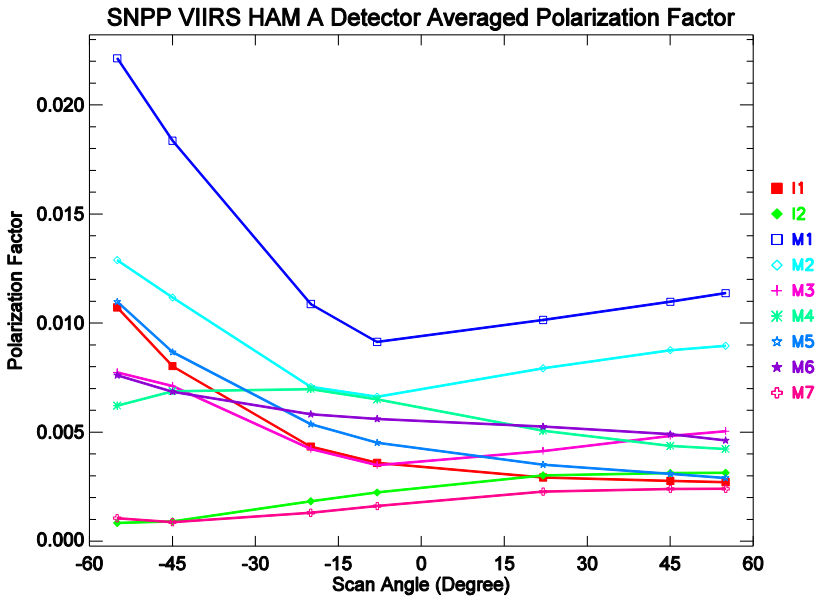

Figure 23. Band averaged polarization factors for SNPP VIIRS (FU1) VisNIR bands HAM A.

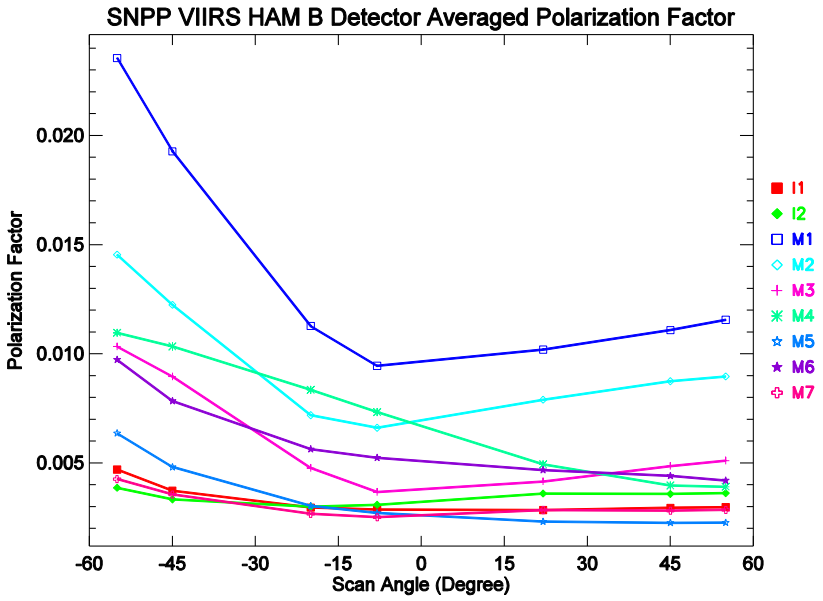

Figure 24. Band averaged polarization factors for SNPP VIIRS (FU1) VisNIR bands HAM B.

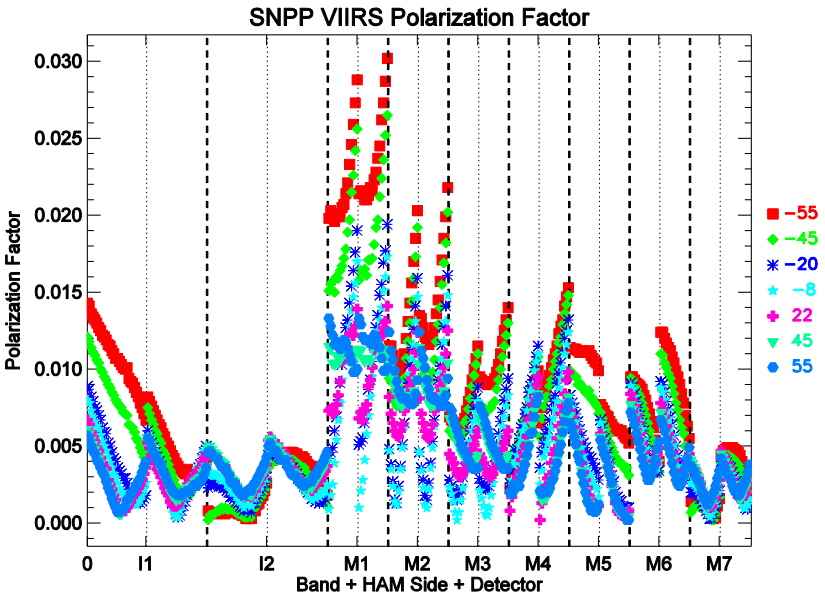

Figure 25. Polarization factors for SNPP VIIRS (FU1) VisNIR bands: Left side of the dotted line for HAM A and the other side for HAM B.

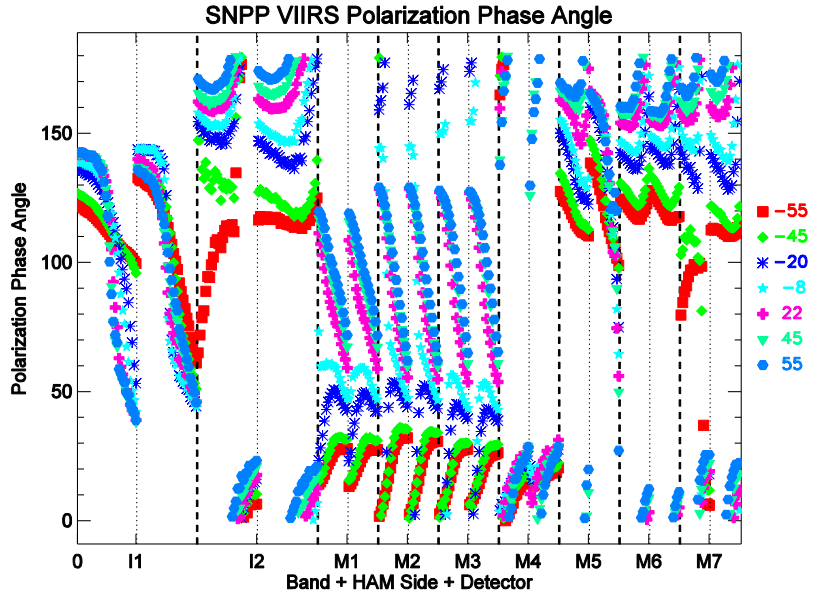

Figure 26. Polarization phase angles for SNPP VIIRS (FU1) VisNIR bands: Left side of the dotted line for HAM A and the other side for HAM B.

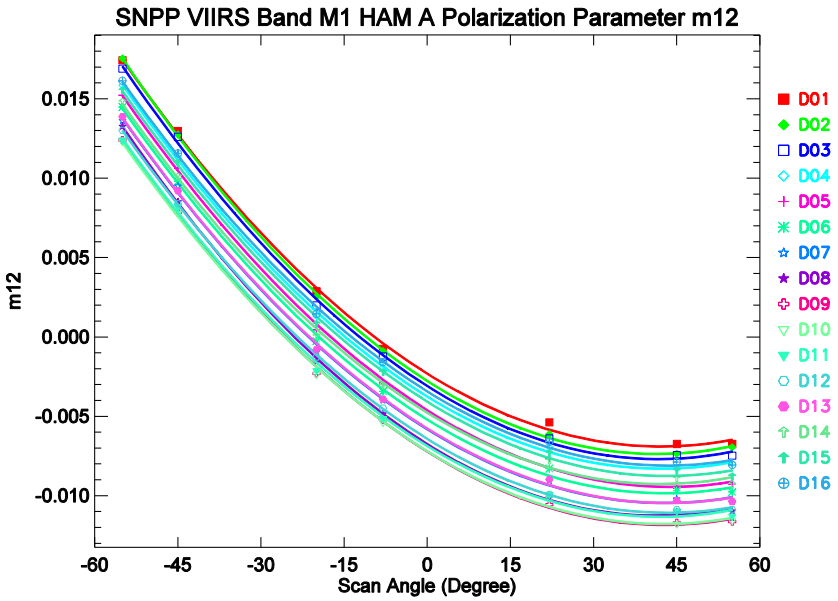

Figure 27. Polarization parameters m12 for SNPP VIIRS (FU1) band M1 HAM A: Left side of the dotted line for HAM A and the other side for HAM B.

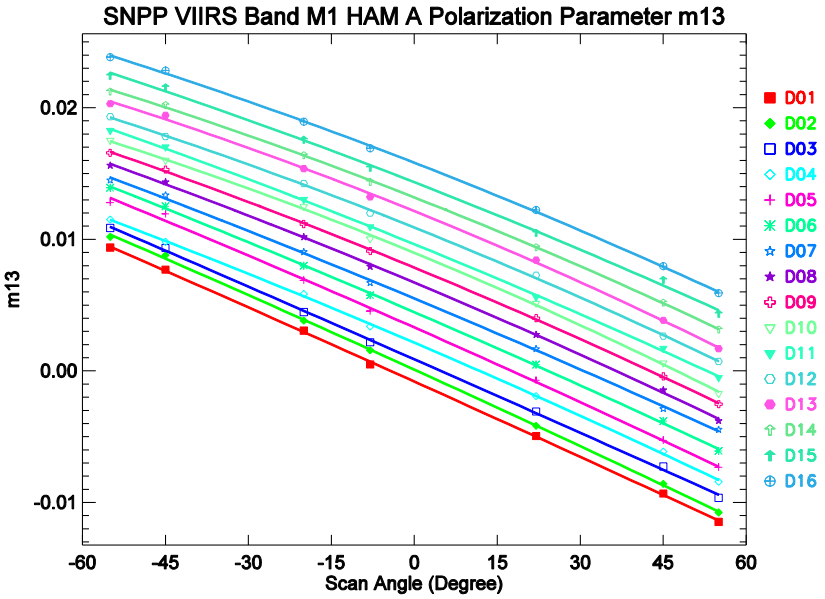

Figure 28. Polarization parameters m13 for SNPP VIIRS (FU1) band M1 HAM A: Left side of the dotted line for HAM A and the other side for HAM B.

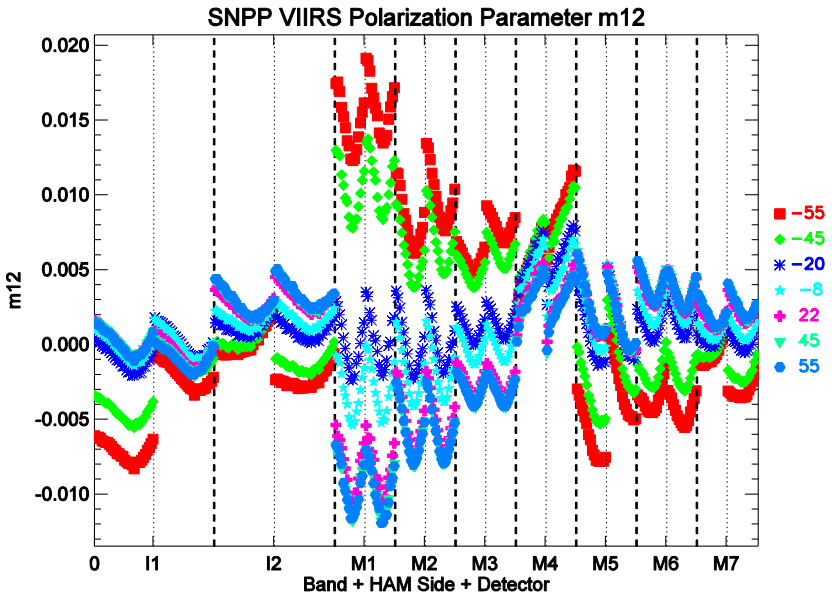

Figure 29. Polarization parameters m12 for SNPP VIIRS (FU1) VisNIR bands: Left side of the dotted line for HAM A and the other side for HAM B.

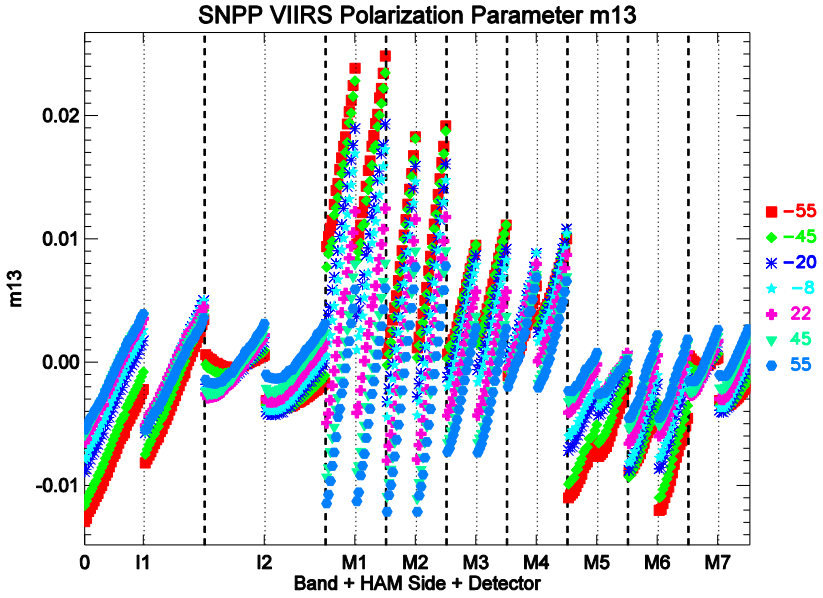

Figure 30. Polarization parameters m13 for SNPP VIIRS (FU1) VisNIR bands: Left side of the dotted line for HAM A and the other side for HAM B.